



River Mobile Armor Layer Induced by Flood

Arlendenovega S. Negara ^{1*}, Cahyono Ikhsan ², RR. Rintis Hadiani ²,
Yusep M. Purwana ²

¹ Doctoral Program in Civil Engineering, Faculty of Engineering, Universitas Sebelas Maret, Surakarta, Jawa Tengah, Indonesia.

² Department of Civil Engineering, Faculty of Engineering, Universitas Sebelas Maret, Surakarta, Jawa Tengah, Indonesia.

Received 03 March 2023; Revised 10 May 2023; Accepted 19 May 2023; Published 01 June 2023

Abstract

The armored layer is crucial for protecting the riverbed. The bed layer of the river is a movable material that protects the material below the surface layer. This study aimed to develop formulas to estimate the thickness of a mobile armor layer with noncohesive materials and establish a correlation between the flow velocity and shear stress under conditions of erosion and sedimentation. The research methods included field measurements, laboratory tests, and numerical simulations. The primary data included grain size gradation profiles, river topography, and flood discharge. The results demonstrated consistency in the behavior of the riverbed under various flood discharge conditions. The fundamental variables affecting the mobile armor thickness included the gradation coefficient (σ_v) and the dimensionless shear stress (τ/τ_c). The fundamental novelty of this study is the derivation of the mobile armor layer thickness, which is influenced by grain size and shear stress. The present findings significantly contribute to the design of more efficient and environmentally friendly riverbed protection rather than rigid structures. These results indicated that erosion and sedimentation were primarily influenced by the flow velocity and the applied shear stress above the riverbed.

Keywords: Armor Layer; Shear Stress; Grain Size; Bed Load; River.

1. Introduction

The research delves into the high frequency of erosion and sedimentation phenomena in rivers and irrigation canals, which incurs high costs for maintaining and constructing canals. This phenomenon has forced policymakers to construct rigid river structures, which are more expensive than unlined channels. Thus, riverbed control work utilizing natural materials is essential for innovating lower river maintenance costs, greater efficiency, and more environmentally friendly river maintenance work. As such, riverbed variations occur naturally in rivers and can affect their environment and hydraulic structures. The variations in riverbed elevation are influenced by the flow velocity [1] and bedload of the sediment transport [2, 3]. Based on the characteristics of the riverbed armor, it can be divided into two types: static and mobile [4, 5]. Although previous research on armor layers should provide a formula for determining the thickness of the armor developed under certain flow conditions, only a few studies have calculated the thickness of the armor layer.

For example, Ikhsan et al. [6] evaluated the thickness of the armor under stationary conditions, and Marion & Fraccarollo [5] presented the formation of mobile armor under steady flow conditions. To date, no study has attempted to derive the thickness of the mobile armor under flood conditions. This research gap inspired us to develop a numerical simulation of mobile armor under flood hydrograph conditions for deriving a formula for the thickness of the mobile armor. In principle, we defined the thickness of the mobile armor as the average thickness of the riverbed alterations in

* Corresponding author: satrianegara@student.uns.ac.id; satrianegara@gmail.com



<http://dx.doi.org/10.28991/CEJ-2023-09-06-05>



© 2023 by the authors. Licensee C.E.J, Tehran, Iran. This article is an open access article distributed under the terms and conditions of the Creative Commons Attribution (CC-BY) license (<http://creativecommons.org/licenses/by/4.0/>).

a single flood hydrograph cycle. To maintain the stability of the river bed, the estimated thickness of the mobile armor is key for the river maintenance work, including gravel augmentation [7] and river restoration [8]. The present study employed numerical simulations using the sediment transport equation with a single hydrograph input under unsteady conditions to derive an overview and formula describing the behavior of the riverbed, especially the thickness of the mobile armor layer formed. The study utilized the HEC-RAS 6.1 software.

The bed layer of a river generally exhibits a larger grain size than the subsurface layer. The process of forming a coarser surface layer to protect the river bed is called armoring [9, 10]. The armoring process poses an essential impact on the channel hydraulics, availability of sediment for sediment transport, determination of the habitat conditions of aquatic species in rivers, geomorphology and turbulence of the river, and degradation of the riverbed [11]. Armoring is more significant in the case of prolonged flooding that reduces the discharge hydrograph compared to the event of a flash flood [9]. The field observations exhibited that a single event of unsteady flow/flood hydrograph can significantly alter the morphology of the riverbed, but no formula has been derived to determine the extent to which the river morphology varies. The texture of the riverbed can transform rapidly under the combined effects of shear stress and grain material availability [12].

The static armor layer is a protective layer at the bottom of rivers/channels formed by flows that only pass finer grains selectively in cases of deficient sediment supply from upstream [13] or when the flow-induced shear stress is less than that required to move the armor grains but is sufficiently large to transport smaller particles [14]. The existing research on static armor indicates that the formation of a layer is influenced by grain size, flow depth, flow rate, sand content, and shear stress [14, 15]. Ikhsan et al. [6] reported that an armor layer is formed when coarser grain materials are arranged in a relatively uniform shape after the maximal transportation of the fine sediments. Moreover, the formation of the channel bottom-surface structure is strongly influenced by grain size and bedload movement, and the thickness of the armor layer is presented as a non-dimensional number.

The mobile armor layer transforms into a protective layer when the variations in the mobility of large and small grains decrease and the percentage of larger grains exposed to flow increases [16, 17]. The concepts of static and mobile armor are explained in Figure 1. The investigation of the mobile armor revealed that its layer structure is not sensitive to the sediment transport rate, except at low magnitudes of transport rate [18, 19]. The formation of the mobile armor layer and the channel bed geometry are strongly influenced by the composition of the grain material in the channel bed. In addition, variations in the shape of the initial surface significantly affect the response to the geometry. Wilcock and DeTemple [11] stated that the mobile armor layer prevalent at low flows can survive at high flows as well. Furthermore, they identified that the armor layers persisting during low flow can simplify the predictions of sediment transport, hydraulic roughness, and habitat disturbance during flood events.





	LOW FLOW	HIGH FLOW
STATIC ARMOUR	 <p>Grain size + Roughness + Complexity +</p>	 <p>Grain size +++ Roughness + Complexity - - -</p>
MOBILE ARMOUR	 <p>Grain size + Roughness ++ Complexity +</p>	 <p>Grain size + Roughness +++ Complexity +</p>

Figure 1. Basic concept of static and mobile armor [18]

The armor layer is a noncohesive natural material located on the riverbed surface in the form of gravel grains. The granules actively merged according to the flow conditions. Therefore, in this study, the material samples from the riverbed were acquired and tested for grain gradation as input for the numerical simulations. To accurately represent the conditions at the instant of the flood, a flood discharge hydrograph calculation was performed based on the actual rainfall data for the last 10 years. Furthermore, numerical simulations were conducted based on grain gradation inputs, river topography, and flood hydrographs under unsteady flow conditions. The unsteady flow condition is a real representation of the river's conditions. Therefore, the present findings are beneficial and purposeful. The existing research literature motivating this study has been adequately studied and referenced, including flood hydrographs, armor layers, shear stress, grain size, and shear strength of grain materials.

1.1. Flood Hydrograph

Flood discharge can control the degree of riverbed armoring. Prior investigation indicated that flooding causes the rupture of armor layers and provides a variable bottom sediment pattern owing to the scavenging flows and successive events [20]. Plumb et al. [21] investigated the impact of hydrograph variations on bedload transport and riverbed morphology. Flood hydrographs with short durations implied that greater bedload transport could result from long periods of above-critical shear stress. In general, sediment supply and hydrograph configuration govern riverbed armoring [22], and a significant amount of sediment is transported in the falling limb hydrograph. The relatively symmetrical shape of the flow hydrograph significantly influences the formation of the riverbed surface, especially in the case of a short hydrograph.

1.2. Mobile Armor Layer and Bed Load Transport

A simple definition of mobile armor is that when the static armor layer breaks and then exposes the sand material underneath, there is a change in the structure of the armor layer, which again closes the gap. This is called mobile armor. Marion et al. [23] demonstrated two groups of grain scales: the conditions for the formation of grain structures tend to be gradual in the form of a stable base and static armor, and second, the conditions for tight formation in the form of mobile armoring are related to strong flow. Generally, the grains in mobile armor are smaller than those in the static armor layer [18]. The formation of the gravel bed clusters apparently influences the formation of armor [24]. Armoring is more significant in the case of a flood over a longer duration that decreases the discharge hydrograph compared to the event of a flash flood [9]. The armoring process at the bottom of the channel is segmented into two processes: surface roughening and cluster formation. The shear stress caused by the flow in the clustering process is greater than that in the roughening process [25].

The formation of mobile armor layers and channel bed geometry are strongly influenced by the composition of the grain material at the bottom of the channel [5]. In addition, the variations in the shape of the initial surface significantly affect the response to the geometry. This study was conducted using a laboratory flume experiment with mixed bimodal and trimodal materials. The response to the basic geometry shows that running on a bimodal sedimentary terrain results in the formation of anti-dunes, whereas the response to the trimodal material exhibits variations in the mobility of the coarse sand material/middle material. Based on empirical evidence, Elgueta-Astaburuaga & Hassan [26] stated that the cycle of degradation and aggradation of the channel/river bottom can be influenced by the upstream sediment supply of escaping sediments and the topography and composition of the channel bottom. Therefore, the surface conditions and sediment availability at the channel bottom are the fundamental factors controlling the sediment transport conditions. Moreover, large-scale cycles of degradation and aggradation are caused by significant fluctuations in the sediment supply, whereas alterations in the local channel bed cause small-scale cycles.

1.3. Shear Stress and Grain Size

In the fields of hydraulic engineering, mechanical engineering, river morphology, and environmental studies, the evaluation of bed shear stress is a challenging task. Lisle & Madej [27] concluded that the flow variations in natural rivers affect the conditions of spatial variation in shear stress by inducing spatial variations in grain size on the surface and subsurface. Chin et al. [10] conducted experimental research on the development of armor layers in nonuniform sediments. As such, nonuniform sediment establishes stable armor layers within a specific range of shear stress. The dimensionless shear critical stress depends on the ratio of the maximum and median sediment particle sizes; the critical armor layer is proportional to the lower limit of a nonuniform material, and the uniform sediments do not bear an armor.

The equilibrium time associated with the diminishing sediment rate in the process of forming the armor layer and geometric roughness is influenced by four parameters: Reynolds number, nondimensional grain median diameter, ratio of the basic shear stress of the channel to the critical shear stress, and ratio of width to the depth of flow [28, 29]. Powell et al. [19] concluded that the structure of the mobile armor layer is insensitive to the transportation rate, except for the low transport rate, which is the nondimensional shear stress of 0.03. Generally, fine materials can transport coarse materials present on the bottom surface of the channel, which can be attributed to the effect of the grain ratio [30]. The model developed by Viparelli et al. [31] demonstrated that the fraction of fine sediments in the uppermost substrate and surface layers can be reduced by flood flow and gravel augmentation.

Wilcock et al. [32] reported that the sand content strongly influences the coarse-grain/gravel transport rate. In mixed conditions of sand and gravel, the increase in the rate of coarse grain transport will rapidly increase across the sand content range of 15–27%. Although the size of the surface grains varies with the sand content, laboratory experimental results revealed a marginal influence of the surface roughening process, including variations in the flow rate and the rate of grain material transport. Moreover, Butler et al. [33] presented a transport model for mixed sand and gravel, which used the full-size distribution of the layers including sand and incorporated the nonlinear effect of the sand content on the gravel-haul rates, which were earlier disregarded in the existing model. Sediments with fine materials or sand tended to form a relatively coarse median grain surface.

1.4. Shear Strength

This study examined the shear strength of the grain material in the armor layer on the riverbed surface to determine its effect. The shear strength of the granular soil can be defined as a function of the normal stress on the failure plane and corresponds to the angular friction of the soil [34]. Shear strength parameters were required to analyze the bearing capacity, slope stability, and thrust. As such, several factors affect the shear strength [35], depending on the relative density, gradation, particle strength, particle size, shape, and degree of saturation. The gravel content primarily influences the shear strength of the coarse material in the gravel-sand mixture. Large-scale direct-shear test equipment is one of the most appropriate methods for determining the shear strength parameters of coarse-grained soils [36]. The shear strength between the bed surface and subsurface layers hypothetically contributes to the development of the armor layer.

2. Research Methodology

The research location is situated on the Krasak River in Magelang Regency, Central Java, and Sleman Regency, Yogyakarta, Indonesia. The Krasak River originates from the active volcano Mount Merapi. A map of the Krasak Watershed is displayed in Figure 2.

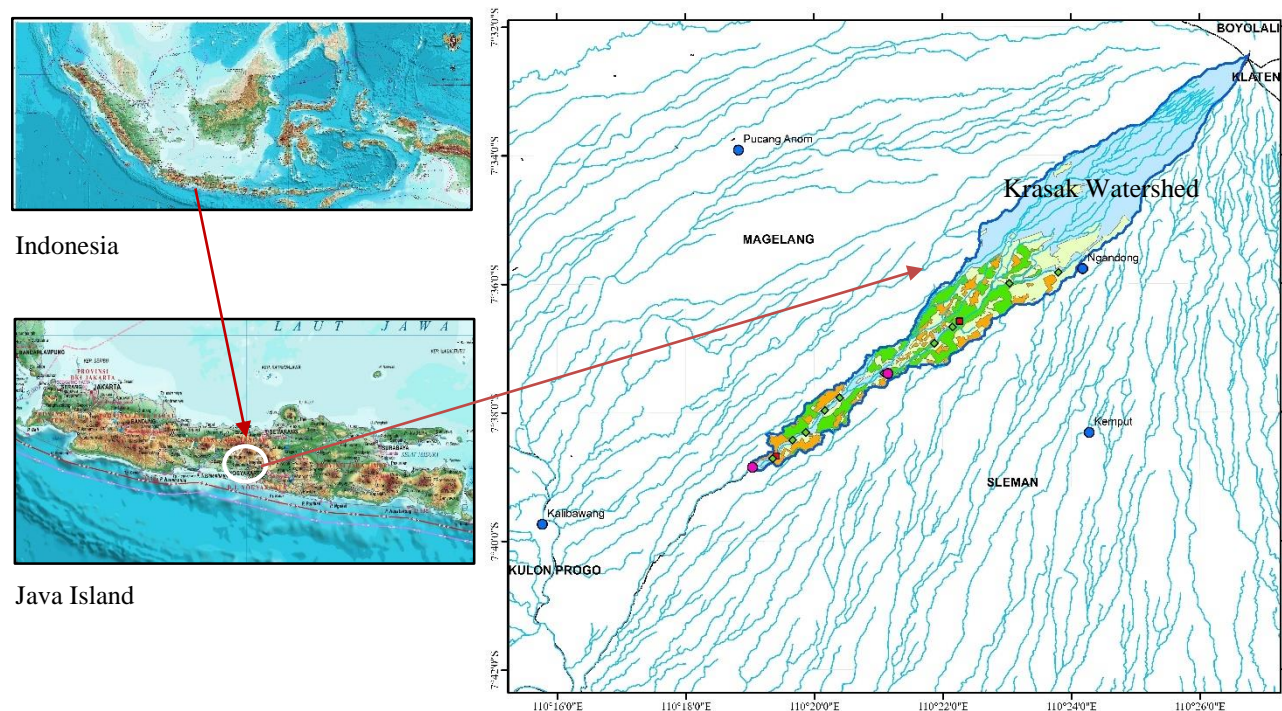


Figure 2. Location of Krasak Watershed

2.1. Research Arrangement

The study aimed to investigate the behavior of the mobile armor layer acting on the surface of the riverbed based on numerical simulations and verify the field measurement results. The study was conducted in four stages, comprising the (1) collection of data on rainfall and river topography, (2) sampling and field measurements, (3) laboratory testing, and (4) numerical simulations using HEC RAS 6.1 software. The study method is schematically illustrated in Figure 3, and the riverbed grain samples were acquired from the Krasak River in the DI Yogyakarta Province, Indonesia. The material from the field was transported to the laboratory for grain gradation and large-scale direct shear tests. Subsequently, the rainfall data and characteristics of the Krasak Watershed were processed into a flood hydrograph based on the GAMA I and SCS Synthetic Unit Hydrograph (SUH) methods. Furthermore, the results of laboratory tests on grain gradation profiles, river topography, and flood hydrographs were employed as inputs in the numerical simulations to record the riverbed response to the flow across various flood discharge conditions.

2.2. Flood Analysis

In terms of river hydraulic analysis, the discharge data are required to devise an overview of the riverbed behavior under flow. As a part of the hydrological analysis, a flow simulation was conducted to determine the riverbed behavior in response to floods. Based on the field surveys and corrected data, no record of water level/discharge was observed in the Krasak River. Moreover, in areas with no runoff records available to derive unit hydrographs, we constructed SUHs based on catchment characteristics to analyze the flood discharge [37]. In particular, the research location was situated at the Krasak River on Java Island in the Magelang Regency and Sleman Regency, Indonesia. Furthermore, the flood discharge hydrograph simulations were performed using two methods: GAMA I (G1–G6) and SCS (S1–S6) SUH.

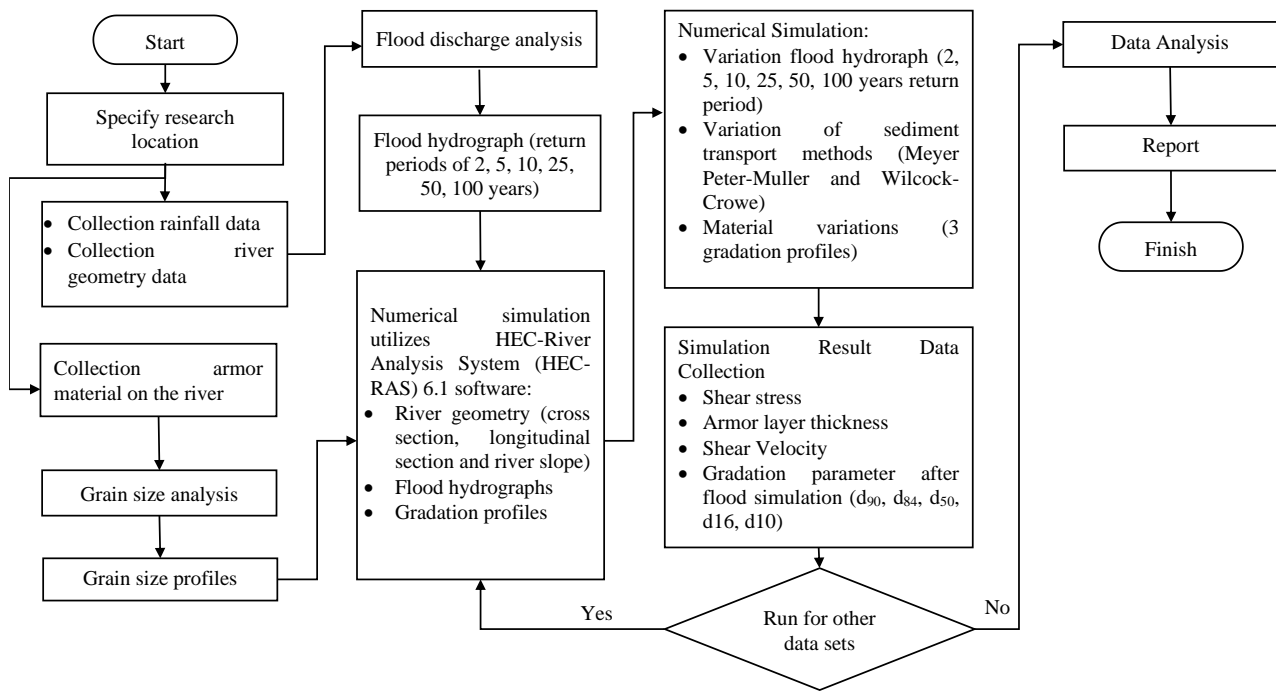


Figure 3. Flowchart of research methodology

2.3. Riverbed Material Analysis

Riverbed material samples were collected from the Krasak River in the Tempel District, Sleman Regency, DI Yogyakarta Province, Indonesia. Materials were collected from three locations by excavating the riverbed. Sampling was conducted by digging the riverbed to obtain a cross-section of the riverbed material. Material sampling was conducted in the middle area of the river, which is an ideal location because the bottom layer of the river experiences high-velocity flow [38]. The riverbed layer of the Krasak River is shown in Figure 4. Based on visual observations, the surface layer has a larger grain size than the layer below it. The surface layer can be referred to as the armor layer, which protects the grain material below [9, 17]. The riverbed material samples were then delivered to the laboratory for grain size analysis. The results of the grain-size analysis of each location were then combined to obtain a single-grain size distribution for each location as an input to the model simulation. The grain-size distribution of the bed material is shown in Figure 5.

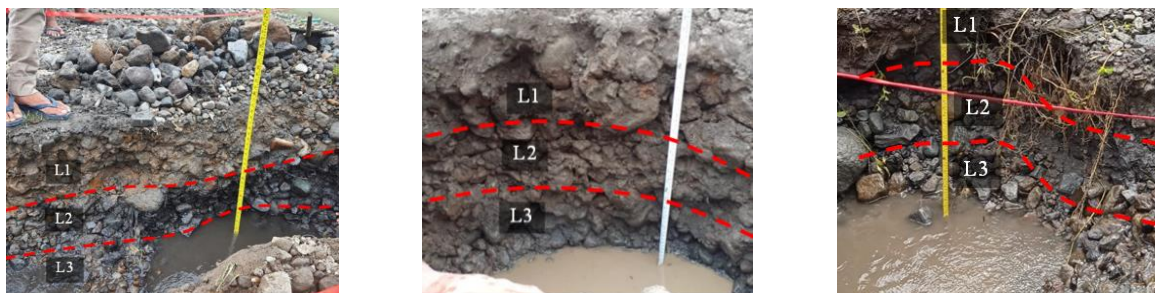


Figure 4. Riverbed layers

2.4. Simulation Parameters

This research was conducted using a numerical simulation model (HEC RAS version 6.1), wherein the input data included cross-sectional data of the 18.93-km-long section of the Krasak River, flood hydrographs, and grain gradation profiles. A combination of sediment transport simulations was performed with 12 variations of flow discharge hydrographs containing flood hydrographs from GAMA I (G1–G6) and the SCS (S1–S6) with 2-, 5-, 10-, 25-, 50-, and 100-year return period. The grain grading input is composed of three material variations (Z1, Z2, and Z3) and two variations of sediment transport using the Meyer–Peter Muller (T1) and Wilcock–Crowe (T2) methods. In total, 72 iterations were simulated to obtain an overview of the response of the riverbed to flood discharge.

In this study, the parameters influencing the formation of the mobile armor layer included shear stress (t), critical shear stress (t_c), average grain diameter (d_{50}), and gradation coefficient (s_g). The results of the numerical simulations highlighted the 16% grain diameter passing through the sieve (d_{a16}), average grain diameter (d_{a50}), 84% grain diameter passing through the sieve (d_{a84}), shear stress (t), critical shear stress (t_c), and thickness of the mobile armor (Ma). In this

case, the thickness of the mobile armor is defined as the average fluctuation in the riverbed elevation because a mobile armor forms by kinematic sorting and fine grain infiltration into the riverbed [17, 18].

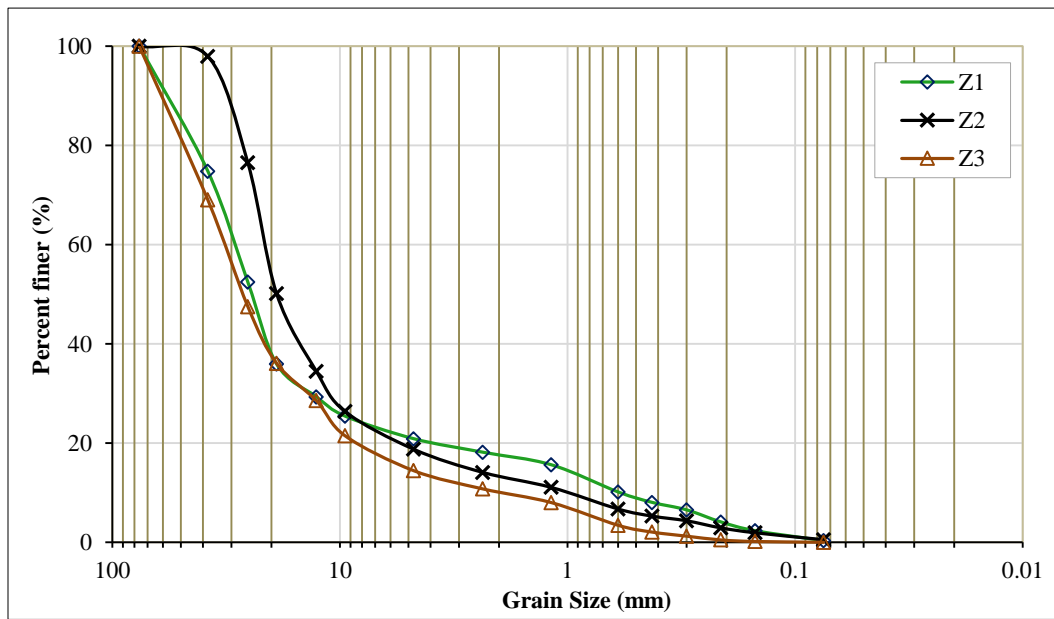


Figure 5. Gradation profiles of riverbed material

2.5. Bedload Transport Analysis

Bedload transport is a component of sediment transport, as the material at the bottom of the channel experiences rolling, sliding, or jumping movements in the vicinity of the channel bottom. Bedload transport is an event that occurs with high variability and is influenced by turbulence [39, 40]. The transport bedload equation was developed by Müller and describes the phenomenon of mobile armor [4]. The Meyer–Müller equation is expressed in Equation 1 [41]:

$$\left(\frac{k_r}{k'_r}\right)^{3/2} \gamma R S = 0,047(\gamma_s - \gamma) d_m + 0,25 \left(\frac{\gamma}{g}\right)^{1/3} \left(\frac{\gamma_s - \gamma}{\gamma_s}\right)^{2/3} g_s^{2/3} \quad (1)$$

where k_r denotes the roughness coefficient, k'_r indicates the roughness coefficient based on grains, γ indicates the unit weight of water, γ_s denotes the unit weight of the sediment, R represents the hydraulic radius, S denotes the energy gradient, d_m indicates the median particle diameter, g denotes the acceleration of gravity, and g_s represents the unit sediment transport rate in weight/time/unit width. The Meyer–Müller equation was derived from laboratory experiments and its applicability was verified based on field tests in rivers with coarse sediment bottoms. The amount of sediment transported was proportional to the difference between the average shear stress and critical grain shear stress.

Wilcock et al. [32] presented a transport model for gravel-sand-sediment mixtures. This model was developed based on laboratory experiments and research in rivers, with a sand content of 16–34% in the riverbed surface [42]. As the grain gradation in the Krasak River was 10.8–18.16%, the Wilcock and Crowe (W-C) formula can be suitably applied in the simulation. W-C defines the W-C surface-based sediment transport formula in terms of nondimensional numbers $\phi = \tau^*/\tau^*_{ri}$ in Equations 2 and 3. The volumetric transport rate formula per unit width is expressed in Equation 4.

$$W_i^* = 0,002\phi^{7,5} \text{ for } \phi < 1.35, \quad (2)$$

$$W_i^* = 14 \left(1 - \frac{0,894}{\phi^{0,5}}\right)^{4,5} \text{ for } \phi \geq 1.35, \quad (3)$$

$$W_i^* = \frac{(s-1)gq_{bi}}{F_i u_*^3}, \quad (4)$$

where ϕ denotes the non-dimensional number of surface-based transported sediments (τ/τ_{ri}), τ indicates the bed shear stress (N/m^2), τ_{ri} denotes the reference bed shear stress (N/m^2), q_{bi} indicates the discharge of the transported grain fraction per unit width, W_i^* accounts for the sediment transported for each grain fraction, F_i denotes the armor grain fraction, ρ_s indicates the sediment density, u_* represents shear velocity, and s denotes the ratio of sediment to water density (ρ_s/ρ). The reference bed shear stress (τ^*_{ri}) was derived from the basic reference shear stress (τ^*_{rm}) on the average grain class, ratio of the particle size of a certain grain class (d_i) on the surface to the average surface grain size (d_{sm}), factor b , and mean surface sand content (F_s), as expressed in Equations 5 to 7:

$$\tau_{ri}^* = \tau_{rm}^* \left(\frac{d_i}{d_{sm}} \right) \quad (5)$$

$$b = \frac{0,67}{1 + \exp\left(1,5 - \frac{d_i}{d_{sm}}\right)} \quad (6)$$

$$\tau_{rm}^* = 0,021 + 0,015 \exp[-20F_s] \quad (7)$$

The bedload transport simulation of the Meyer–Müller and Wilcock–Crowe equations generated 36 equations corresponding to the mobile armor layer thickness. These equations were analyzed by conducting an optimization process with the Excel solver. Principally, we attempted to derive a general equation that can accurately estimate the thickness of the mobile armor layer protecting the underlying riverbed layer.

3. Results and Discussion

3.1. Thickness of Mobile Armor Layer

The numerical simulations were executed with 12 datasets of flood hydrographs, three datasets of grain size distributions, and two methods of the sediment transport equation. The flood hydrographs were sourced from GAMA I (G1–G6) and SCS (S1–S6), containing 2-, 5-, 10-, 25-, 50-, and 100-year return periods. The GAMA I SUH was initially developed based on research on flood data and simulations on Java Island [37]. In particular, we utilized the SCS method considering that it is widely used in research and applications and provides an accurate estimation of flood hydrographs [43]. The grain size distributions were obtained from the Krasak River samples (Z1, Z2, and Z3). These three sets of riverbed materials were sampled from three distinct locations on the Krasak River, representing the general characteristics of the river based on the statistical homogeneity test. The sediment transport was evaluated using the Meyer–Müller (T1) and Wilcock–Crowe (T2) equations. The Meyer–Müller equation is a prominent method for evaluating sediment transport loads. The Wilcock–Crowe equation was developed from the bed surface gradation material of the flume and river with a sand content of 6–34% and is represented by the sand content of the Krasak River in the range of 10.8–18.16%.

The variations in the tendencies of the mobile armor in the simulation results obtained using the MP-M and W-C sediment transport methods are presented in Figure 6. The thickness of the mobile armor with respect to the nondimensional shear stresses in the W-C method was steeper than that in the M-PM method, implying that the amount of sediment transported by the W-C method is more sensitive to the increase in shear stress associated with the grain size and mobile armor layer thickness (Figure 6). This finding demonstrated that the W-C bedload equation provided a larger amount of bedload transport than that predicted by the MP-M formula. Therefore, an optimization analysis of the two graphs was separately performed. Based on numerical modeling, Cordier et al. [44] reported that the W-C (2003) formula [33] provides a more relevant fractional and total sediment transport rate than the classic MP-M formula. However, Bettess & Frangipane [45] claimed that the MP-M formula has more accuracy than other experimental data methods, even if the initial assumption considers excessive sediment transport rates.

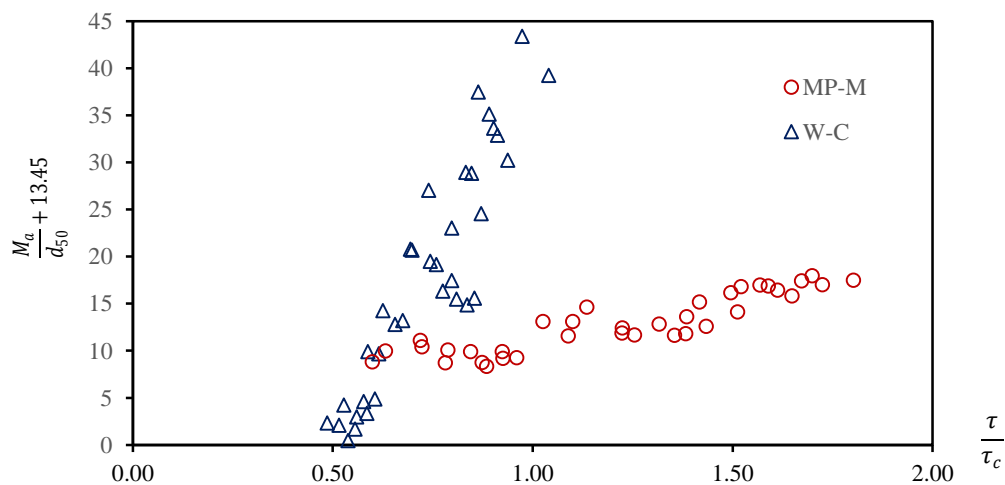


Figure 6. Correlation of dimensionless shear stress and the thickness of mobile armor layer

In total, 72 iterations of the numerical simulation were conducted to obtain an overview of the riverbed response to the flood discharge hydrograph. These 72 equations were processed using Excel to obtain an optimization formula representing a series of functions. Hypothetically, the equations generated by the MP-M and W-C simulations can be

applied to certain grain types or flow characteristics. An example of the combinations executable on three material datasets (Z1-3), six combinations of flood hydrograph datasets (G1-6), and the M-PM transport sediment formula (T1) is presented in Table 1.

Table 1. Simulation of mobile armor layer thickness for T1, G1–6, and Z1–3 data sets

Running	Maximum discharge in m ³ /s	Maximum flow velocity in m/s	Mean diameter of riverbed sediment in mm (D_{b50})	The mean diameter of active/armor layer in mm (D_{a50})	Shear stress induced by flow in N/m ² (τ_0)	Critical shear stress of the river bed in N/m ²	Coefficient of the gradation (σ_g)	$E = \left[\frac{M_a}{d_{50}} + \theta \right] - \alpha \left[\frac{\tau}{\tau_c} \right]^\beta [\sigma_g]^\chi$
T1G1Z1	173.89	2.99	24.45	23.91	20.41	21.52	3.43	$E_1=9.20-\alpha[0.93]^\beta [3.43]^\chi$
T1G1Z2	173.89	3.27	18.93	20.50	29.82	18.46	5.39	$E_2=16.42-\alpha[1.61]^\beta [5.39]^\chi$
T1G1Z3	173.89	3.46	26.85	21.55	33.99	19.40	4.62	$E_3=17.98-\alpha[1.70]^\beta [4.62]^\chi$
T1G2Z1	162.35	3.20	24.45	24.32	20.04	21.89	3.40	$E_4=8.34-\alpha[0.88]^\beta [3.40]^\chi$
T1G2Z2	162.35	3.56	18.93	20.59	29.08	18.53	4.60	$E_5=16.97-\alpha[1.57]^\beta [4.60]^\chi$
T1G2Z3	162.35	3.56	26.85	21.64	33.47	19.47	4.63	$E_6=17.41-\alpha[1.67]^\beta [4.63]^\chi$
T1G3Z1	150.62	3.23	24.45	24.79	19.46	22.31	3.21	$E_7=9.93-\alpha[0.84]^\beta [3.21]^\chi$
T1G3Z2	150.62	3.52	18.93	20.60	28.24	18.54	5.23	$E_8=16.82-\alpha[1.52]^\beta [5.23]^\chi$
T1G3Z3	150.62	3.58	26.85	21.69	32.08	19.52	4.48	$E_9=16.88-\alpha[1.59]^\beta [4.48]^\chi$
T1G4Z1	134.47	3.27	24.45	25.57	18.57	23.02	3.12	$E_{10}=8.71-\alpha[0.78]^\beta [3.12]^\chi$
T1G4Z2	134.47	3.48	18.93	20.60	26.53	18.54	5.19	$E_{11}=12.60-\alpha[1.43]^\beta [5.19]^\chi$
T1G4Z3	134.47	3.63	26.85	21.79	30.13	19.62	4.48	$E_{12}=16.15-\alpha[1.50]^\beta [4.48]^\chi$
T1G5Z1	121.25	3.30	24.45	26.21	17.62	23.59	3.05	$E_{13}=10.44-\alpha[0.72]^\beta [3.05]^\chi$
T1G5Z2	121.25	3.48	18.93	20.80	24.30	18.72	5.15	$E_{14}=12.84-\alpha[1.32]^\beta [5.15]^\chi$
T1G5Z3	121.25	3.67	26.85	21.92	28.77	19.73	4.36	$E_{15}=15.17-\alpha[1.42]^\beta [4.36]^\chi$
T1G6Z1	100.20	3.32	24.45	27.59	15.95	24.83	2.93	$E_{16}=9.98-\alpha[0.63]^\beta [2.93]^\chi$
T1G6Z2	100.20	3.49	18.93	21.40	21.19	19.26	5.01	$E_{17}=14.64-\alpha[1.14]^\beta [5.01]^\chi$
T1G6Z3	100.20	3.60	26.85	22.17	24.95	19.96	4.22	$E_{18}=11.89-\alpha[1.22]^\beta [4.22]^\chi$

Powell et al. [19] demonstrated that the variables tested in the mobile armor events included shear stress consistency, critical shear stress, and grain size. Essential specifications of grain size have been applied to evaluate sediment transport in river gradation coefficients [46]. In this study, the key parameters influencing the formation of the mobile armor layer included the shear stress (τ), critical shear stress (τ_c), average grain diameter (d_{50}), and gradation coefficient (σ_g). The thickness function of the mobile armor (M_a) can be mathematically expressed through the analysis of dimensionless numbers, as expressed in Equation 8.

$$M_a = f(\tau, \tau_c, d_{50}, \sigma_g) \quad (8)$$

Furthermore, the dimensionless formula is expressed in Equation 9.

$$\frac{M_a}{d_{50}} = f\left[\frac{\tau}{\tau_c}, \sigma_g\right] \quad (9)$$

Based on the simulation results, Equation 9 was modified for field applications, as expressed in Equations 10 and 11:

$$\frac{M_a}{d_{50}} - \theta = \left[\frac{\tau}{\tau_c}\right] [\sigma_g] \quad (10)$$

$$\frac{M_a}{d_{50}} - \theta = \alpha \left[\frac{\tau}{\tau_c}\right]^\beta [\sigma_g]^\chi \quad (11)$$

where $\frac{M_a}{d_{50}}$ is dimensionless mobile armor layer thickness, θ is mobile armor thickness coefficient, τ = bed shear stress, τ_c is critical shear stress, σ_g is gradation coefficient is $\sqrt{d_{84}/d_{16}}$, α , β , χ is coefficient of optimization, M_a is thickness of the mobile armor layer, d_{50} is average grain diameter, and θ is coefficient of nondimensional shear stress difference. Thereafter, an optimization analysis was conducted to derive the values of α , β , and χ in the dimensionless mobile armor layer formula expressed in Equations 12.

$$\left[\frac{M_a}{d_{50}} + \theta\right] = \alpha \left[\frac{\tau}{\tau_c}\right]^\beta [\sigma_g]^\chi \quad (12)$$

The variations between the points on the curve (E) in Figure 6 are highlighted in Equation 13:

$$E = \left[\frac{M_a}{d_{50}} + \theta \right] - \alpha \left[\frac{\tau}{\tau_c} \right]^\beta [\sigma_g]^\chi \quad (13)$$

with $\theta=13.45$.

As observed, the coarsening process of the material corresponds to shear stress. A consistent coarsening process occurs when the shear stress caused by the flow exceeds the critical shear stress. The results of the optimization analysis using the Excel solver yielded the optimization coefficient values listed in Table 2. Based on the analysis results, the equation generated based on the MP-M sediment transport method (Equation 14) can be used for relatively larger grain sizes compared with the W-C method formula (Equation 15).

Table 2. Optimization Results of α , β , and χ value

Sediment transport method	α	β	χ
MP-M	7.74	0.10	0.70
W-C	13.14	2.46	0.10

$$\frac{M_a}{d_{50}} = \left[7.74 \left[\frac{\tau}{\tau_c} \right]^{0.1} [\sigma_g]^{0.7} \right] - 13.45 \quad (14)$$

with boundary conditions: $\tau > \tau_c$; $3.39 \leq d_{50} \leq 43.98$ mm; $2.93 \leq \sigma_g \leq 5.56$; $\tau \geq 14.87$ N/m²

$$\frac{M_a}{d_{50}} = \left[13.14 \left[\frac{\tau}{\tau_c} \right]^{2.46} [\sigma_g]^{0.1} \right] - 13.45 \quad (15)$$

with boundary conditions: $\tau > \tau_c$; $1.13 \leq d_{50} \leq 29.1$ mm; $5.65 \leq \sigma_g \leq 6.3$; $\tau \geq 8.91$ N/m²

To estimate the thickness of the mobile armor, Equations 14 and 15 can be practically executed for designing the armor layer as riverbed protection. As evaluated from the equations, mobile armor materials can be sourced from local gravel and sand with a minimum diameter. The mobile armor layer condition occurs when the shear stress on the riverbed exceeds the critical shear stress. Conversely, the size of the static armor material is the minimum diameter at which the shear stress occurring on the bed is smaller than the critical shear stress. Therefore, the diameter of the mobile armor material can be smaller than that of the static armor material, thereby facilitating its field implementation.

3.2. Simulation Accuracy and Verification

To verify and control the sensitive parameters during the numerical simulation, we conducted field measurements of the velocity profile of the Krasak River. The field measurements were conducted at the same three locations as the riverbed sediment sampling locations. The logarithmic law of the velocity profile method could accurately calculate the shear stress [47]. The correlation between the results of the field shear stress measurements and numerical simulations is displayed in Figure 7.

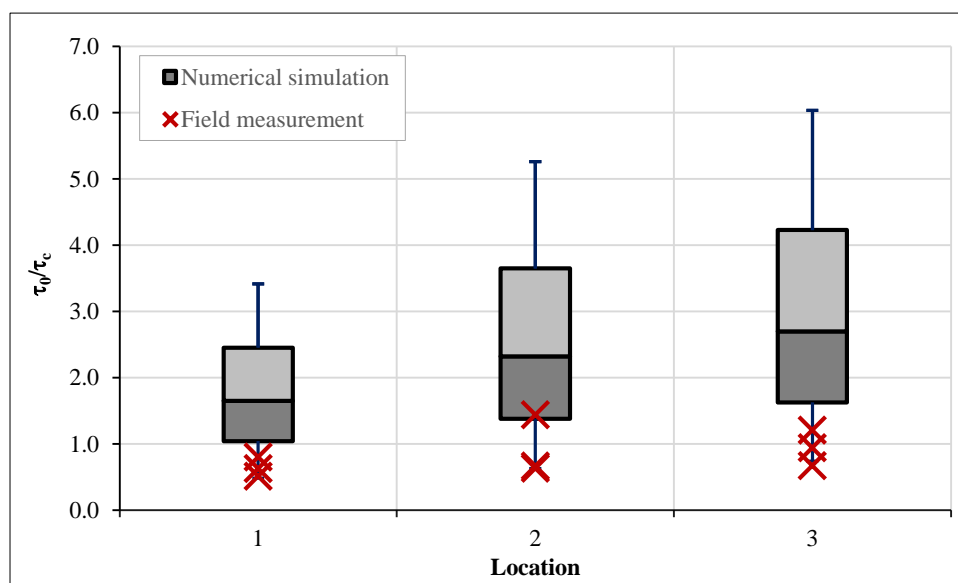


Figure 7. Dimensionless shear stress generated by flow obtained by numerical simulation and field measurement

The boxes plotted in Figure 7 represent the 25th, 50th, and 75th percentiles, and the whiskers in the upper and lower layers correspond to the maximum and minimum values of the numerical simulation results for the dimensionless shear

stress, respectively. The dimensionless shear stress evaluated from the simulation results was consistent with that of the field measurements. Moreover, the standard deviation values ranged from 0.08–0.32. The shear stress of the flow to the riverbed was relatively sensitive to the characteristics of the surface bed materials.

3.3. Velocity

Debris flows with particle collisions dominating the shear stress are referred to as "stony debris flows," whereas those dominated by the turbulent shear stresses are referred to as "turbulent muddy debris flows," and those dominated by viscoplastic pressures are called "viscous debris flows" [48]. The correlation of the velocity coefficient values with the nondimensional relative depth is depicted in Figure 8 based on the previous studies on the Nojiri River by the Ohsumi Work Office [48], the Mizhunasi River by Hirano et al. [49], and the Kamikamihori River and Jianjia Gully by Takahashi [50]. The data were compared with those obtained from a numerical simulation at Kali Krasak. Based on the relative depth and velocity coefficients, the findings demonstrate that the Krasak River exhibits characteristics identical to those of the Jiangjia River, containing viscous-type debris flows. For instance, it bears less resistance than the stony-type debris flow in the Kamikamihori Ravine. Takahashi [50] stated that stone-type debris flows can occur only at relatively shallow depths ranging from 20 to 30. The Krasak River follows a viscous debris flow with a relative depth of more than 30, similar to the Nojiri and Mizunashi rivers. Based on this analysis, mobile armor can occur in viscous-type debris flows with relative depths larger than 30.

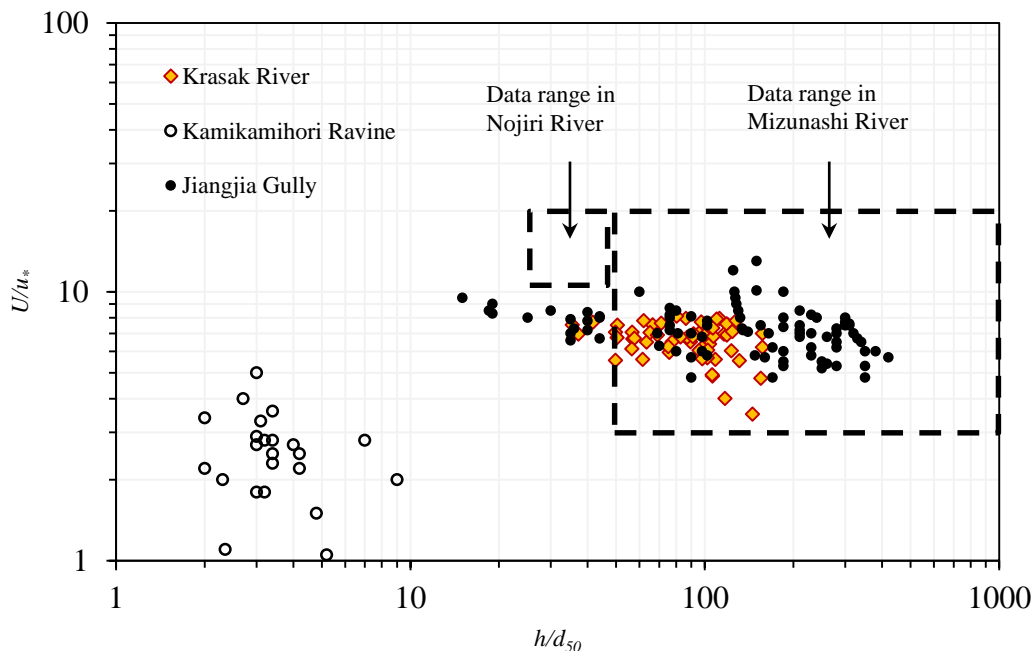


Figure 8. Characteristics of dimensionless velocity correspond to relative depth (Previous study by Takahashi [50] compared with Krasak River)

3.4. Shear Stress

The flow velocity affected the scour process at the bottom of the channel, which was protected by the armor layer. The maximum scour depth on a riverbed surface with a finer particle size was greater than that on a channel bed surface with a coarser grain diameter [51]. In Figure 9, the regression line indicates the correlation between the shear stress and flow velocity. According to the Newtonian fluid law, the shear stress on the bed surface is proportional to the flow velocity along the boundary [52]. Negara et al. [53] stated that erosion occurs if the shear stress is less than 21 N/m². Otherwise, the deposition occurs at shear stresses greater than 21 N/m². Therefore, by determining the correlation between velocity and shear stress (Figure 9), the flow velocity limits causing sedimentation and erosion can be determined. In principle, the mobile armor moves to the bottom of the channel to cause erosion temporarily and replenishes the erosion into deposition. Therefore, if riverbed protection is to be achieved, then theoretically, the value of the shear stress is maintained at ~21 N/m², which is heaped with an average grain size, as illustrated in the optimization results in Figure 9.

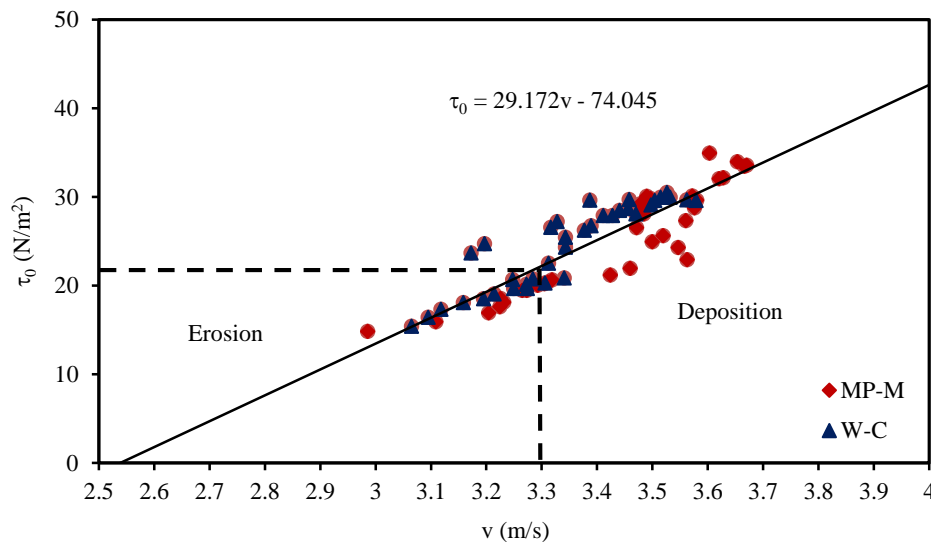


Figure 9. Correlation between shear stress and flow velocity

3.5. Soil Shear Strength

Large-scale direct-shear testing was performed in a soil mechanics laboratory. The tests were conducted according to the principles listed in SNI 3420:2016 concerning the direct shear strength test method for unconsolidated and non-drained soils. Based on the Unified Soil Classification System, gravel is defined as a grain material with a size ranging from 4.76–75 mm [54]. The results of the grain material gradation test from the Krasak River indicated that the number of grains measuring 4.76–75 mm ranged from 81.84–89.2%. Therefore, this material can be categorized as gravel. However, conducting the shear strength test for gravel materials is relatively challenging using conventional triaxial test equipment and direct shear tests. Therefore, the shear strength test can utilize large-scale direct shear instruments [55]. As illustrated in Figure 10, the large-scale direct shear results signified an increase in the shear stress as the load or stress was applied to the material specimen. If a specific shear stress occurs at the bottom of a river, the horizontal displacement can be estimated to correspond to the movable riverbed of the mobile armor layer. The behavior of the shear ratio of the Krasak riverbed material with $\sigma_v = 0.64 \text{ kg/cm}^2$ exhibited a similar behavior with sand ($D_r = 0.22$) [56]. Therefore, a substantial increase in the shear stress ratio (τ/σ_v) contributes to bed resistance.

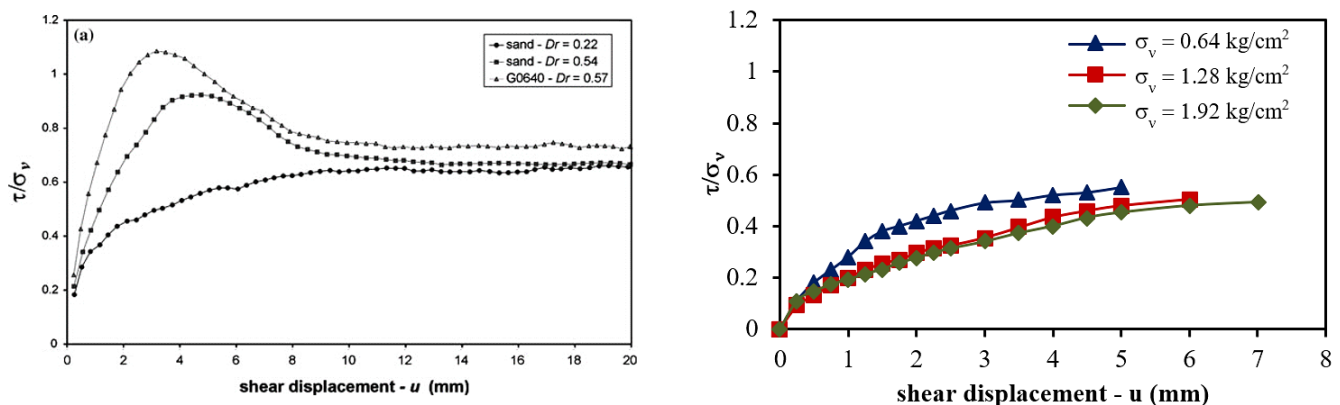


Figure 10. Shear strength ratio corresponds to shear displacement. (a) Previous study by Simoni & Houlsby (2006); (b) Large-scale direct shear test of Krasak riverbed material

4. Conclusions

This study conducted field measurements, laboratory tests, and numerical simulations to investigate the effects of grain size and shear stress on the thickness of mobile armors with noncohesive materials. As such, the movement of material in a riverbed is a natural process resulting from sediment transport. Nonetheless, examining the movable layers of the armor is considered more relevant according to field conditions than the discussion of static armor layers. Therefore, this study focused on determining the thickness of the mobile armor through numerical experiments. The major findings of this study are stated as follows:

- The mobile armor thickness estimation formulas are expressed in Equations 14 and 15. As observed, the thickness

of the mobile armor layer is influenced by the gradation coefficient (σ_v) corresponding to the material grain size and dimensionless shear stress (τ_0/τ_c). The equation for estimating the thickness of the mobile armor derived herein can facilitate engineers in estimating the grain size requirement such that the riverbed elevation conditions are maintained and do not undergo significant alterations. The maintained riverbed elevation can reduce the potential for damage to river structures owing to the threat of degradation and scouring.

- The amount of sediment transport calculated by the Wilcock–Crowe (2003) method was more sensitive to the increase in shear stress associated with the flow velocity than that evaluated by the M-PM method. This conclusion is crucial for selecting the calculation method to be employed for sediment transport simulations according to field observations and considerations of safety factors for estimating the bedload transport.
- The correlation between shear stress and flow velocity (Figure 9) can describe the behavioral conditions of the riverbed, which experiences aggradation or degradation to facilitate policymakers in river improvements.
- The sediment transport estimation formula derived using the MP-M method can be used for relatively larger grain sizes compared to the formula obtained from the W-C method.
- A consistent coarsening process occurs when the shear stress caused by the flow exceeds the critical shear stress.

The present findings exhibit consistency in the behavior of the riverbed under various flood discharge conditions. The equation for estimating the thickness of the mobile armor derived herein contributes to the design and calculation of more efficient riverbed protection compared with rigid structures and static armor. A limitation of this study is that only two methods were used for the sediment transport analysis. In such cases, various methods may yield varying effects of shear stress on the armor layers. The limitations of this study include challenges for further investigation, and future studies should assess more appropriate methods for estimating the thickness of the mobile armor layer.

5. Declarations

5.1. Author Contributions

Conceptualization, A.S.N., and C.I.; methodology, A.S.N.; software, A.S.N.; validation, A.S.N., and C.I.; formal analysis, A.S.N.; investigation, A.S.N.; resources, A.S.N.; data curation, A.S.N.; writing—original draft preparation, A.S.N.; writing—review and editing, A.S.N., C.I., R.H., and Y.M.P.; visualization, A.S.N.; supervision, C.I., R.H., and Y.M.P.; project administration, A.S.N.; funding acquisition, A.S.N. All authors have read and agreed to the published version of the manuscript.

5.2. Data Availability Statement

The data presented in this study are available on request from the corresponding author.

5.3. Funding

The authors received no financial support for the research, authorship, and/or publication of this article.

5.4. Conflicts of Interest

The authors declare no conflict of interest.

6. References

- [1] Cooper, J. R., & Tait, S. J. (2009). Water-worked gravel beds in laboratory flumes - A natural analogue? *Earth Surface Processes and Landforms*, 34(3), 384–397. doi:10.1002/esp.1743.
- [2] Yager, E. M., Kenworthy, M., & Monsalve, A. (2015). Taking the river inside: Fundamental advances from laboratory experiments in measuring and understanding bedload transport processes. *Geomorphology*, 244, 21–32. doi:10.1016/j.geomorph.2015.04.002.
- [3] Zhang, S., Zhu, Z., Peng, J., He, L., & Chen, D. (2021). Laboratory study on the evolution of gravel-bed surfaces in bed armoring processes. *Journal of Hydrology*, 597, 125751. doi:10.1016/j.jhydrol.2020.125751.
- [4] Hunziker, R. P., & Jaeggi, M. N. R. (2002). Grain Sorting Processes. *Journal of Hydraulic Engineering*, 128(12), 1060–1068. doi:10.1061/(asce)0733-9429(2002)128:12(1060).
- [5] Marion, A., & Fraccarollo, L. (1997). Experimental investigation of mobile armoring development. *Water Resources Research*, 33(6), 1447–1453. doi:10.1029/97WR00705.
- [6] Ikhsan, C., Permana, A. S., & Negara, A. S. (2022). Armor Layer Uniformity and Thickness in Stationary Conditions with Steady Uniform Flow. *Civil Engineering Journal (Iran)*, 8(6), 1086–1099. doi:10.28991/CEJ-2022-08-06-01.
- [7] Pasternack, G. B. (2010). Gravel/Cobble Augmentation Implementation Plan (GAIP) for the Englebright Dam Reach of the Lower Yuba River, CA. US Army Corps of Engineers, Washington, United States.

- [8] Tranmer, A. W., Caamaño, D., Clayton, S. R., Giglou, A. N., Goodwin, P., Buffington, J. M., & Tonina, D. (2022). Testing the effective-discharge paradigm in gravel-bed river restoration. *Geomorphology*, 403. doi:10.1016/j.geomorph.2022.108139.
- [9] Vázquez-Tarrio, D., Piégay, H., & Menéndez-Duarte, R. (2020). Textural signatures of sediment supply in gravel-bed rivers: Revisiting the armor ratio. *Earth-Science Reviews*, 207(November 2019), 103211. doi:10.1016/j.earscirev.2020.103211.
- [10] Chin, C. O., Melville, B. W., & Raudkivi, A. J. (1994). Streambed armoring. *Journal of Hydraulic Engineering*, 120(8), 899-918. doi:10.1061/(ASCE)0733-9429(1994)120:8(899).
- [11] Wilcock, P. R., & DeTemple, B. T. (2005). Persistence of armor layers in gravel-bed streams. *Geophysical Research Letters*, 32(8), 1–4. doi:10.1029/2004GL021772.
- [12] Mrokowska, M. M., & Rowinski, P. M. (2019). Impact of unsteady flow events on bedload transport: A review of laboratory experiments. *Water (Switzerland)*, 11(5). doi:10.3390/w11050907.
- [13] Koll, K., Koll, K., & Dittrich, A. (2010). Sediment transport over static armor layers and its impact on bed stability. *River Flow 2010*, 929-936.
- [14] Ikhsan, C., Rahajo, A., & Legono, D. (2014). The formation of static armor layer. *International Journal of Civil & Environmental Engineering*, 14, 19-23.
- [15] Curran, J. C., & Waters, K. A. (2014). The importance of bed sediment sand content for the structure of a static armor layer in a gravel bed river. *Journal of Geophysical Research: Earth Surface*, 119(7), 1484–1497. doi:10.1002/2014JF003143.
- [16] Parker, G., Klingeman, P. C., & McLean, D. G. (1982). Bedload and size distribution in paved gravel-bed streams. *Journal of the Hydraulics Division - ASCE*, 108(HY4), 544–571. doi:10.1061/jyceaj.0005854.
- [17] Orrú, C., Blom, A., & Uijttewaalt, W. S. J. (2016). Armor breakup and reformation in a degradational laboratory experiment. *Earth Surface Dynamics*, 4(2), 461–470. doi:10.5194/esurf-4-461-2016.
- [18] Mao, L., Cooper, J. R., & Frostick, L. E. (2011). Grain size and topographical differences between static and mobile armor layers. *Earth Surface Processes and Landforms*, 36(10), 1321–1334. doi:10.1002/esp.2156.
- [19] Powell, D. M., Ockelford, A., Rice, S. P., Hillier, J. K., Nguyen, T., Reid, I., Tate, N. J., & Ackerley, D. (2016). Structural properties of mobile armors formed at different flow strengths in gravel-bed rivers. *Journal of Geophysical Research: Earth Surface*, 121(8), 1494–1515. doi:10.1002/2015JF003794.
- [20] Vericat, D., Batalla, R. J., & Garcia, C. (2006). Breakup and reestablishment of the armor layer in a large gravel-bed river below dams: The lower Ebro. *Geomorphology*, 76(1–2), 122–136. doi:10.1016/j.geomorph.2005.10.005.
- [21] Plumb, B. D., Juez, C., Annable, W. K., McKie, C. W., & Franca, M. J. (2020). The impact of hydrograph variability and frequency on sediment transport dynamics in a gravel-bed flume. *Earth Surface Processes and Landforms*, 45(4), 816–830. doi:10.1002/esp.4770.
- [22] Hassan, M. A., Egozi, R., & Parker, G. (2006). Experiments on the effect of hydrograph characteristics on vertical grain sorting in gravel bed rivers. *Water Resources Research*, 42(9). doi:10.1029/2005WR004707.
- [23] Marion, A., Tait, S. J., & McEwan, I. K. (2003). Analysis of small-scale gravel bed topography during armoring. *Water Resources Research*, 39(12). doi:10.1029/2003WR002367.
- [24] Heays, K. G., Friedrich, H., & Melville, B. W. (2014). Laboratory study of gravel-bed cluster formation and disintegration. *Water Resources Research*, 50(3), 2227–2241. doi:10.1002/2013WR014208.
- [25] Zhang, S., Zhu, Z., Peng, J., He, L., & Chen, D. (2021). Laboratory study on the evolution of gravel-bed surfaces in bed armoring processes. *Journal of Hydrology*, 597(October 2020). doi:10.1016/j.jhydrol.2020.125751.
- [26] Elgueta-Astaburuaga, M. A., & Hassan, M. A. (2019). Sediment storage, partial transport, and the evolution of an experimental gravel bed under changing sediment supply regimes. *Geomorphology*, 330, 1–12. doi:10.1016/j.geomorph.2018.12.018.
- [27] Lisle, T. E., & Madej, M. A. (1992). Spatial variation in armoring in a channel with high sediment supply. *Dynamics of gravel-bed rivers*, 277-293, John Wiley and Sons, Hoboken, United States.
- [28] Berni, C., Perret, E., & Camenen, B. (2018). Characteristic time of sediment transport decrease in static armor formation. *Geomorphology*, 317, 1–9. doi:10.1016/j.geomorph.2018.04.004.
- [29] Bertin, S., & Friedrich, H. (2018). Effect of surface texture and structure on the development of stable fluvial armors. *Geomorphology*, 306, 64–79. doi:10.1016/j.geomorph.2018.01.013.
- [30] Venditti, J. G., Dietrich, W. E., Nelson, P. A., Wydzyga, M. A., Fadde, J., & Sklar, L. (2010). Mobilization of coarse surface layers in gravel-bedded rivers by finer gravel bed load. *Water Resources Research*, 46(7), 1–10. doi:10.1029/2009WR008329.

- [31] Viparelli, E., Gaeuman, D., Wilcock, P., & Parker, G. (2011). A model to predict the evolution of a gravel bed river under an imposed cyclic hydrograph and its application to the Trinity River. *Water Resources Research*, 47(2). doi:10.1029/2010WR009164.
- [32] Wilcock, P. R., Kenworthy, S. T., & Crowe, J. C. (2001). Experimental study of the transport of mixed sand and gravel. *Water Resources Research*, 37(12), 3349–3358. doi:10.1029/2001WR000683.
- [33] Butler, D., May, R., & Ackers, J. (2003). Self-cleansing sewer design based on sediment transport principles. *Journal of Hydraulic Engineering*, 129(4), 276–282. doi:10.1061/(ASCE)0733-9429(2003)129.
- [34] Das, B. M. (2019). *Advanced soil mechanics*. CRC Press, London, United Kingdom. doi:10.1201/9781351215183.
- [35] Islam, M. A., Badhon, F. F., & Abedin, M. Z. (2017). Relation between Effective Particle Size and Angle of Internal Friction of Cohesionless Soil. *Proceedings from International Conference on Planning, Architecture and Civil Engineering*, RUET, 9-11 February, 2017, Rajshahi, Bangladesh.
- [36] Hamidi, A., Azini, E., & Masoudi, B. (2012). Impact of gradation on the shear strength-dilation behavior of well graded sand-gravel mixtures. *Scientia Iranica*, 19(3), 393–402. doi:10.1016/j.scient.2012.04.002.
- [37] Triatmodjo, B. (2015). *Applied Hydrology* (5th Ed.). Beta Offset Yogyakarta, Yogyakarta, Indonesia. (In Indonesian).
- [38] Technical Supplement 13A. (2007). *Guidelines for Sampling Bed Material*. Part 654, National Engineering Handbook, United States Department of Agriculture, Washington, United States.
- [39] Melville, B. W. (1999). Book Review: *Fluvial Hydraulics: Flow and Transport Process in Channels of Simple Geometry*. *Journal of Hydraulic Engineering*, 125(10), 1109–1110. doi:10.1061/(asce)0733-9429(1999)125:10(1109).
- [40] López, R., Vericat, D., & Batalla, R. J. (2014). Evaluation of bed load transport formulae in a large regulated gravel bed river: The lower Ebro (NE Iberian Peninsula). *Journal of Hydrology*, 510, 164–181. doi:10.1016/j.jhydrol.2013.12.014.
- [41] HEC-RAS. (2021). *River Analysis System Hydraulic Reference Manual*. Hydrological Engineering Center, US Army Corps of Engineering, Washington, United States.
- [42] HEC-RAS. (2021). *River Analysis System Hydraulic Reference Manual*. Hydrological Engineering Center, US Army Corps of Engineering, Washington, United States.
- [43] Shatnawi, A., & Ibrahim, M. (2022). Derivation of flood hydrographs using SCS synthetic unit hydrograph technique for Housha catchment area. *Water Supply*, 22(5), 4888–4901. doi:10.2166/ws.2022.169.
- [44] Cordier, F., Tassi, P., Claude, N., van Bang, D. P., Crosato, A., & Rodrigues, S. (2016). Numerical modelling of graded sediment transport based on the experiments of Wilcock and Crowe (2003). *Proceedings of the XXIIIrd TELEMAT-MASCARET User Conference 2016*, 11-13 October, 2016, Paris, France.
- [45] Bettess, R., & Frangipane, A. (2003). A one-layer model to predict the time development of static armor. *Journal of Hydraulic Research*, 41(2), 179–194. doi:10.1080/00221680309499960.
- [46] Almasalmeh, O., Saleh, A. A., & Mourad, K. A. (2021). Soil erosion and sediment transport modelling using hydrological models and remote sensing techniques in Wadi Billi, Egypt. *Modeling Earth Systems and Environment*, 8(1), 1215–1226. doi:10.1007/s40808-021-01144-1.
- [47] Naderi, M., Afzalimehr, H., Dehghan, A., Darban, N., Nazari-Sharabian, M., & Karakouzian, M. (2022). Field Study of Three-Parameter Flow Resistance Model in Rivers with Vegetation Patch. *Fluids*, 7(8), 284. doi:10.3390/fluids7080284.
- [48] Ohsumi Work Office. (1988). *Debris Flow at Sakurajima*. Ohsumi Work Office, Kyushu Regional Construction Bureau, Ministry of Construction, Tokyo, Japan.
- [49] Hirano, M., Hashimoto, H., Kouno, M., Onda, K., & Park, K. (1999). Field Measurements of Debris Flows in the Mizunashi and Nakao Rivers on Mt Unzen-Hugen Dake. *Doboku Gakkai Ronbunshu*, 1999(635), 49–65. doi:10.2208/jscej.1999.635_49.
- [50] Takahashi, T. (2009). A Review of Japanese Debris Flow Research. *International Journal of Erosion Control Engineering*, 2(1), 1–14. doi:10.13101/ijec.2.1.
- [51] Pandey, M., Chen, S. C., Sharma, P. K., Ojha, C. S. P., & Kumar, V. (2019). Local scour of armor layer processes around the circular pier in non-uniform gravel bed. *Water (Switzerland)*, 11(7), 1–10. doi:10.3390/w11071421.
- [52] Jobson, H. E., & Froehlich, D. C. (1987). *Basic principles of open channel hydraulics*. Developments in Water Science, Elsevier, Amsterdam, Netherlands. doi:10.1016/S0167-5648(08)70006-6.
- [53] Negara, A. S., Ikhsan, C., Hadiani, R. R., & Yusep, M. (2022). Effect of bed shear stress on the mobile armor layer at the riverbed. In *The 8th International Conference of EACEF 2022*, Switzerland.

- [54] United States department of Agriculture. (2012). Chapter 3 Engineering Classification of Earth Materials. Part 631 National Engineering Handbook, Natural Resources Conservation Service, United States Department of Agriculture, Washington, United States.
- [55] Yunatci, A. A., & Çetin, K. Ö. (2022). Large Scale Direct Shear Box Tests on Gravels. *Teknik Dergi / Technical Journal of Turkish Chamber of Civil Engineers*, 33(1), 11617–11623. doi:10.18400/tekderg.606816.
- [56] Simoni, A., & Houlsby, G. T. (2006). The direct shear strength and dilatancy of sand-gravel mixtures. *Geotechnical and Geological Engineering*, 24(3), 523–549. doi:10.1007/s10706-004-5832-6.